THESIS FOR THE DEGREE OF LICENTIATE OF ENGINEERING

Railway wheel steel behaviour upon thermo-mechanical loadings

ERIKA STEYN

CHALMERS
UNIVERSITY OF TECHNOLOGY

Department of Industrial and Materials Science

CHALMERS UNIVERSITY OF TECHNOLOGY

Gothenburg, Sweden 2022

Railway wheel steel behaviour upon thermo-mechanical loadings
ERIKA STEYN

© ERIKA STEYN, 2022.

Technical report no IMS-2022-9
Department of Industrial and Materials Science
Division of Engineering Materials
Chalmers University of Technology
SE-412 96 Gothenburg
Sweden
Telephone + 46 (0)31-772 1000

Chalmers Reproservice
Gothenburg, Sweden 2022

Aan my Hartsmense: vir al die liefde, ondersteuning en gebede.

“Ek is tot alles in staat deur Hom wat my krag gee. Nietemin het julle goed gedoen deur my in my moeilike omstandighede by te staan.” Filippense 4:13-14.

Railway wheel steel behaviour upon thermo-mechanical loadings

ERIKA STEYN
Department of Industrial and Materials Science
Chalmers University of Technology

Abstract

Optimised railway maintenance techniques such as rail grinding and milling, or rail repair welding, are vital to more sustainable rail networks. As demands on the railway increases, the need to better understand the material behaviour during local heating events occurring during maintenance is amplified. Other heating events can occur during operation, for instance during severe block braking. This thesis provides insight into thermal damage resulting from these local heating events on railway wheels, which can lead to altered mechanical properties and changed residual stresses.

The material behaviour of the ferritic-pearlitic railway wheel steel ER7T was studied during severe block braking (i.e., slow heating and cooling) at peak temperatures varying between 300 °C and 650 °C. The thermal dilatation was restricted to different degrees between free expansion and full restriction. This study thus explores the combined effect of thermal and mechanical cycling on the mechanical properties and material structure. The experimental results from the thermo-mechanical testing were also used to validate a new constitutive material model for use in FE models to predict severe block braking.

The second part of the thesis explored the effect of rapid heating and cooling events on the microstructure and residual stress state of railway wheel steel. Localised heating using laser scanning with additive manufacturing equipment was compared to the heating done by scanning with laser welding equipment. This study thus investigated the similarities of different rapid heating (high temperature) processes and the effect of process parameter variations.

The results can be used to provide insight into the material behaviour of railway steels during local heating events. Furthermore, it can support the development of more accurate simulations for both operation and maintenance processes.

Keywords: railway wheel steel, pearlitic microstructure, thermo-mechanical fatigue, residual stress, repair welding, severe block braking

Preface

The research presented in this thesis is carried out at the Department of Industrial and Materials Science at Chalmers University of Technology between June 2019 and August 2022. The research project MU36, “Material characteristics in welding and other local heating events”, is part of the ongoing activities within the National Centre of Excellence CHARMEC – Chalmers Railway Mechanics (www.chalmers.se/charmec). The study has been partially funded from the European Union’s Horizon 2020 research and innovation programmes in the projects In2Track2 and In2Track3 under grant agreement numbers 826255 and 101012456.

Appended papers

Paper I **Thermo-mechanical response of near-pearlitic steel heated under restriction of thermal expansion.** E. Steyn, J. Ahlström. *Manuscript*.

Author contribution: Planning, execution, and analysis of TMF experiments (same experiments as used in Paper II) and performed subsequent room temperature hardness testing and microstructural analysis. Contributed to the planning and writing of the paper.

Paper II **Thermomechanical testing and modelling of railway wheel steel.** E. Voortman Landström, E. Steyn, J. Ahlström, T. Vernersson. *Submitted to Int. Journal of Fatigue*.

Author contribution: Planned the TMF test cycles with the first author and then executed the experiments (same experiments as used in Paper II). Subsequent room temperature hardness testing and heat treatment was done. Contributed to writing of the paper, with focus on the materials and experimental sections.

Paper III **Simulation of repair welding on pearlitic railway steel using additive manufacturing equipment**. E. Steyn, J. Ahlström. Proceedings of the *12th International Conference on Contact Mechanics and Wear of Rail/Wheel Systems, Melbourne, Australia, 2022*

Author contribution: Planning and execution of laser scanning experiments, as well as subsequent residual stress measurements, room temperature hardness testing and microstructural analysis. The author was also responsible for planning and writing of the paper, and oral presentation of the work at the 2022 Contact Mechanics Conference.

Report not appended to this thesis:

D3.1 – section 2.1.3. Rail machining strategies. E. Steyn, B. Paulsson, A. Ekberg. *Manuscript deliverable for In2Track3. 2022.*

List of abbreviations and acronyms

AM	Additive manufacturing
bct	body-centered tetragonal (crystal structure)
DSA	Dynamic strain ageing
EDM	Electric discharge machining
EU	European Union
FEGSEM	Field emission gun scanning electron microscope
LB-PBF	Laser-based powder bed fusion
LCC	Life cycle cost
LCF	Low cycle fatigue
LW	Laser welding
MMA	Manual metal arc welding
RCF	Rolling contact fatigue
SAW	Submerged arc welding
SEM	Scanning electron microscope/ microscopy
TMF	Thermo-mechanical fatigue
XRD	X-ray diffraction
ZST(E)	Zero-stress test/ Zero-stress test evaluation
ZTS	Zero total strain

Table of contents

ABSTRACT I
PREFACE II
APPENDED PAPERS II
LIST OF ABBREVIATIONS AND ACRONYMS III
INTRODUCTION 1
1.1 Railways and the European Green Deal 1
1.2 Project background 1
1.3 Aim and research objectives 2
RAILWAY OPERATIONS AND MAINTENANCE 5
2.1 Railway operations and damage mechanisms 5
2.2 Railway maintenance 6
RAILWAY MATERIALS 7
3.1 Railway materials 7
3.2 Microstructures of interest 9
3.3 Fatigue behaviour 13
RESEARCH METHODOLOGY 15
4.1 Samples 15
4.2 Thermo-mechanical testing 16
4.3 Laser scanning 20
4.4 Heat treatment 21
4.5 Hardness 21
4.6 Microscopy 22
4.7 Residual stress measurements 22
ANALYSES AND RESULTS 23
5.1 Thermo-mechanical behaviour of railway wheel steel 23
5.2 Effect of rapid heating and cooling on residual stress state 24
5.3 Microstructural analyses 25
CONCLUDING REMARKS 27
6.1 Research objectives as addressed in appended papers 27
6.2 Future work 27
ACKNOWLEDGEMENTS 29
REFERENCES 30

INTRODUCTION

1.1 Railways and the European Green Deal

In 2021, the European Union (EU) committed to a 55 % reduction in carbon emissions by 2030, and to achieving a carbon-neutral status by 2050 as part of the European Green Deal [1]. Transport accounts for nearly one third of the EU's greenhouse gas emissions, while rail transport contributes a mere 0.4 % (see Figure 1) [2,3]. In 2019, 52 % of all goods transported in the EU was by road, while only 12 % was transported by rail. For the same year, only 7 % of all European travel was by train [3].

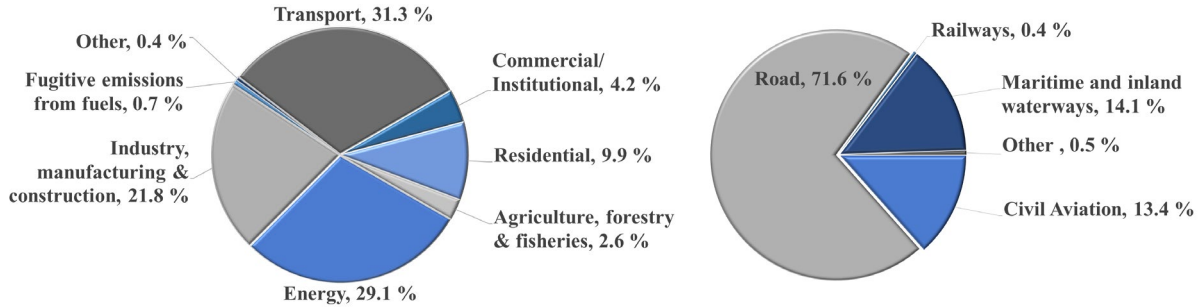

Figure 1: CO_2 emissions by sector (left) and by transport mode (right) [3]

To achieve climate neutrality by 2050, transport emissions need to be reduced by 90 %. An important initiative is the development of a sustainable trans-European railway network, with the main goals being to triple high-speed rail traffic and double rail freight traffic. This expansion represents a quick win in emission reduction goals. Infrastructure improvements and expansion will have to focus on reducing life cycle cost (LCC) and improving end-user affordability [2,4].

Infrastructure development inevitably comes with technical challenges, such as higher demands for maintenance, both qualitative and quantitative, while reducing maintenance time slots. Standardisation and improved predictive models can be utilised to improve traffic management and maintenance activities. Programmes such as Horizon Europe provide the resources and framework for research and development needed to achieve these milestones and overcome challenges and facilitates collaboration between industry and various research areas [4].

1.2 Project background

A sustainable rail network will require effective maintenance techniques and optimised maintenance strategies. Subtractive surfacing techniques such as rail grinding and milling are used to remove material to restore damaged or worn rail and wheel contact surfaces. Repair welding is an additive technique for localised repairs, but additional research is required to optimise the mechanical and microstructural properties of the repaired section. These repair techniques induce local heating which can result in

thermal damage, leading to altered mechanical properties and residual stresses. Similarly, local heating events during operation can result in the degradation of the microstructure, with detrimental effects on the mechanical performance. Heat treatment during production can be used to customise the steel for railway wheels and rails to obtain specific desirable mechanical properties, such as high strength, good wear resistance or improved fatigue resistance.

In pearlitic railway steels, local heating events can result in phase transformations of the affected material. Different phases can have different temperature dependent properties (for example thermal expansion, density, or mechanical properties), that can result in residual stresses or the localisation of strains during subsequent loading. Ultimately, these phase transformations can lead to defects in the rail and wheel surfaces, which may result in increased maintenance interventions.

Maintenance strategies aim to maximise component life and minimise the life cycle cost (LCC). Conventional repair methods can be optimised through the application of, for instance, controlled heat input to achieve beneficial heat treatment, or optimising welding fillers and additives to customise specific material compositions that will improve the mechanical properties of the repaired component. New repair methods, such as laser welding and additive manufacturing are evolving fast through continuous research and testing, but scientific evidence will have to prove these new technologies as superior before they can replace the existing and proven repair procedures. The local heating events during operation, such as friction in the wheel-rail contact area during braking, can cause thermal damage like what is seen in the material behaviour during heat inducing maintenance processes.

Previous studies considered the behaviour of pearlitic steels after exposure to plastic straining and elevated temperatures respectively, and the combination of strain and temperature for the isothermal case. The results provide insights into the effects of different thermal processes, such as rail welding [5–7], laser cladding [8,9] and contact friction heating [10–14]. Studies that combine different research areas can provide new insights that can improve predictive models of thermal processes during both rail operations and maintenance.

1.3 Aim and research objectives

This thesis work aims at characterising the material behaviour of railway wheel steel during these high temperature processes, with special consideration for thermo-mechanical cycling (combined thermal and mechanical loading) and the influence of process parameters.

The main objectives include:

- Characterising the material behaviour of pearlitic railway wheel steel (ER7T) during thermo-mechanical loadings imitating severe block braking; investigating the effect of the degree of thermal dilatation restriction on the mechanical properties and material structure.

- Experimental validation of a new numerical model for severe block braking.
- Characterisation of the effect of rapid heating and cooling events on the microstructure and residual stress state of ER7T material to support development of welding simulations [15].

The outcomes of this research will build on the understanding of pearlitic material behaviour during local heating events and can contribute to the development of improved maintenance guidelines and more accurate predictive models of high-temperature processes.

The theoretical background for this thesis work is summarised in sections two and three. Section 2 discusses degradation mechanisms and maintenance techniques used within the railway industry, and Section 3 provides an overview of typical railway materials and their fatigue behaviour. Section 4 discusses the research methodology used to obtain the results of the appended papers, as summarised and discussed in Section 5. Section 6 provides a snapshot of the current position of this research.

RAILWAY OPERATIONS AND MAINTENANCE

2.1 Railway operations and damage mechanisms

Distinction is made between passenger, freight, or mixed traffic on railways. The deterioration of the track is influenced by the type and amount of traffic, as well as the dynamic loads during operation. These loads can be affected by the train weight, travel speed and the wheel-rail contact [16]. The typical shape of this contact area, along with key parts of the rail and wheelset, is shown in Figure 2.

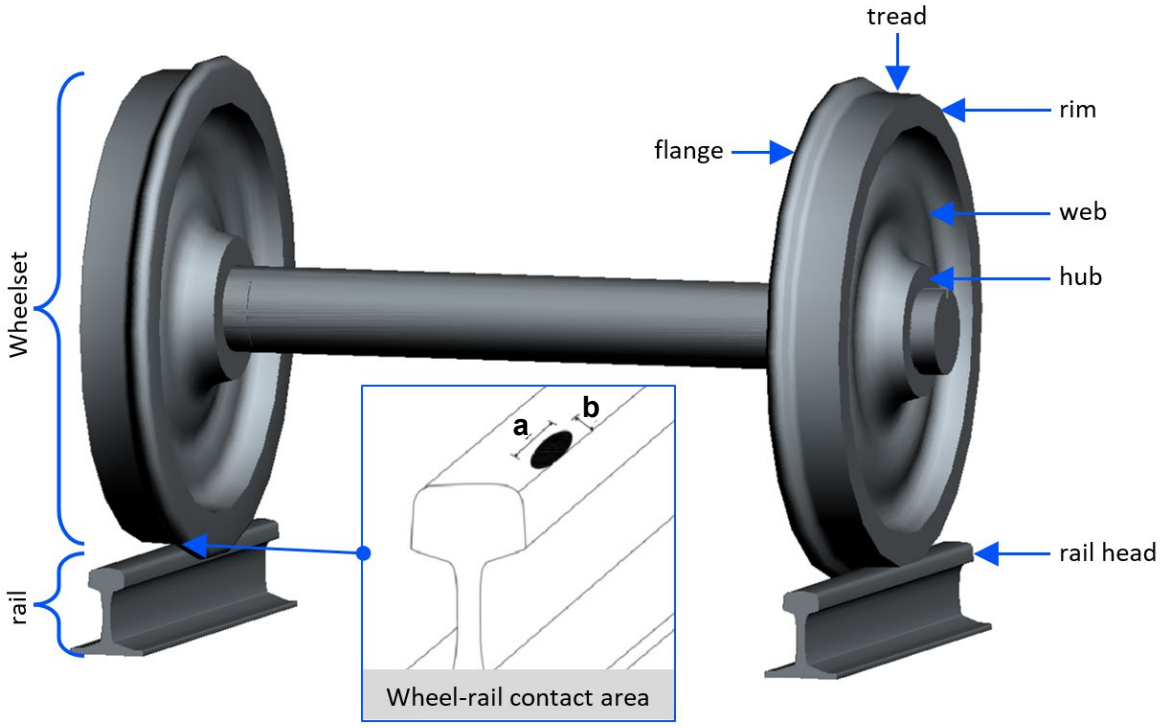

Figure 2: Components of a wheelset with a typical S-type wheel on a UIC 60E1 profile rail, as well as the wheel-rail contact area (from [17] *under CC by 4.0)*

As the wheel and rail are worn during operation, the shape of this contact-area changes. This can have detrimental dynamic effects due to changes in the contact loading [18,19]. The highest loads experienced by the wheel, is in the flange and tread surface. Frictional forces in the wheel-rail contact area, combined with rolling contact fatigue, can cause wear and crack formation on both the wheel and rail surface. This is aggravated during block braking or traction, resulting in wheel sliding, material yielding and undesirable phase transformations. High temperatures can be reached in the surface layers of the different components – this is caused by atomic bonds that are broken during plastic deformation. As the wheel slides along the rail, the wheel is exposed to more heat for a longer duration, decreasing the temperature gradient and allowing for larger volumes to austenitise. As soon as the wheel starts rolling, the heat dissipates, and martensite can form due to high cooling rates. These phase

transformations in the wheel tread surface (discussed in Section 3) can be detrimental to the mechanical properties and introduce residual stresses, increasing the risk of cracking or other surface damage [10,20–23].

Surface damage, such as plastic deformation, crack development and thermal damage, can alter the profile geometries of the wheel and rail. This in turn can increase the contact loads, induce vibrations that aggravate the dynamic loading and lead to more severe surface deterioration [12,19,24]. Ultimately, this increases the need for maintenance.

2.2 Railway maintenance

Surfacing technologies, such as rail grinding and milling, are used to remove surface damage and to reprofile the wheel tread or rail head; this is intended to improve the wheel-rail contact. Typically, a wheel can be reprofiled two to five times during its lifetime, depending on the severity of the damage. More severe damage, including subsurface cracks, would require higher material removal. Some preventive maintenance strategies require frequent removal of a thin surface layer, for example the scraping technique employed on railway wheels used in Dutch railways [19]. Subtractive machining processes remove the damaged surface layer and expose new material with somewhat different properties to that of the original surface.

Additive repair techniques, such as repair welding, can be used to address localised damage. Rail repair welding is done by cutting out the damaged section and rebuilding the rail head layer by layer. Finally, the profile is restored by grinding off the excess weld deposits. Welding is typically not allowed on railway wheels in practice, but methods to restore the flange or wheel tread to sufficient dimensions (overlay welding) are being investigated [25–27]. Multi-pass fusion welding processes, such as manual metal arc welding (MMA) and submerged arc welding (SAW), are typically used for railway repairs [19,27]. Rail welding techniques used for joining of rails, such as thermite or flash butt welding, has a high heat input. In contrast, rail repair welding has a low heat input and small weld beads are used, resulting in higher cooling rates. Each subsequent weld pass causes heat treatment of the previous weld deposit layer, gradually changing the material property of that layer. This results in localised thermal loads, which provide necessary tempering to a more ductile behaviour but can also cause unwanted microstructural changes (like local bainitic or martensitic regions) and mechanical property gradients [15,19].

Both subtractive and additive maintenance techniques require well defined procedures based on the actual material behaviour during different thermal processes. The material behaviour during railway maintenance is similar to that during operations, which could be used to establish universal principles.

3.1 Railway materials

Table 1: Chemical composition (maximum wt %) of common railway materials

Element [wt %, max]	C	Si	Mn	Mo[a,b]	Cr[a]	Ni[a,b]	S	P	V	Cu[b]	Al	N	Fe	Sn[b]	Sb[b]	Ti[b]	Nb[b]	H[d,e]
ER7	0.52	0.40	0.80	0.08	0.30	0.30	0.02	0.02	0.06	0.30	-	-	Balance	-	-	-	-	2.50
ER8	0.56	0.40	0.80	0.08	0.30	0.30	0.02	0.02	0.06	0.30	-	-		-	-	-	-	2.50
R260[c]	0.82	0.60	1.25	0.02	0.15	0.10	0.03	0.03	0.03	0.15	0.0	0.01		0.03	0.02	0.03	0.01	2.50
R260Mn	0.77	0.62	1.75	0.02	0.15	0.10	0.03	0.03	0.03	0.15	0.0	0.01		0.03	0.02	0.03	0.01	2.50

a) For ER7 and ER8: Mo, Cr and Ni combined cannot exceed 0.5 wt %
b) Mo, Ni, Cu, Sn, Sb, Ti and Nb are considered residual elements in rail steel R260 and R260Mn. Here, the following applies: (Cu + 10 Sn) ≤ 0.35 wt % AND (Cr + Mo + Ni + Cu + V) ≤ 0.35 wt %
c) This compositional data is valid for all rail profiles over 27 kg/m. However, EN 13674 Part 1 (rails 46 kg/m and heavier) have an additional requirement that oxygen content cannot exceed 0.002 % (ppm) by mass.
d) Unit: ppm (10^{-6}) by mass, maximum.
e) These values apply to category 2 wheels. For category 1 wheels (traffic speed >200 km/h), this is reduced to 2.00.

3.1.1. Railway wheel steel

Railway wheels are commonly made from medium carbon steels with a pearlitic microstructure. In Europe, the most common grades are ER7 and ER8, with standardised compositions according to EN 13262 as shown in Table 1, although other grades are also used in different regions [28–30]. ER7 is suitable for most applications, whereas ER8 is typically used in high-demand applications [28,31]. These materials have a near-pearlitic microstructure with 10 % free ferrite close to the virgin wheel surface, slightly higher for the ER7 material [32].

Railway wheel design and production

Railway wheels should be designed for strength, good wear and thermal resistance, and with noise characteristics in mind. However, different properties are required in different sections (indicated in Figure 3a) of the wheel [28,29,33]. The web should be able to handle the mechanical loads imposed by the rolling stock, whilst resisting fatigue and thermal stresses. This can be managed by altering the curvature and thickness of the web. The wheel rim on the other hand is susceptible to tread wear, rolling contact fatigue (RCF) and thermal damage, which is mitigated by increasing the hardness of the rim during production. Rim chilling (shown in Figure 3b) is a heat treatment process during which only the rim is in contact with agitated water to create a hard, fine-pearlitic surface. The material for these wheels is then designated with a T following the steel grade, e.g., ER7T.

EN 13262 further distinguishes between category 1 and 2 wheels, where category 1 wheels are used for high speed (over 200 km/h) rails and category 2 wheels for travel speeds up to and including 200 km/h. Some differences are that category 1 wheels have higher requirements on the homogeneity of the wheel rim hardness and a lower defect size as measured by non-destructive testing (NDT) [28].

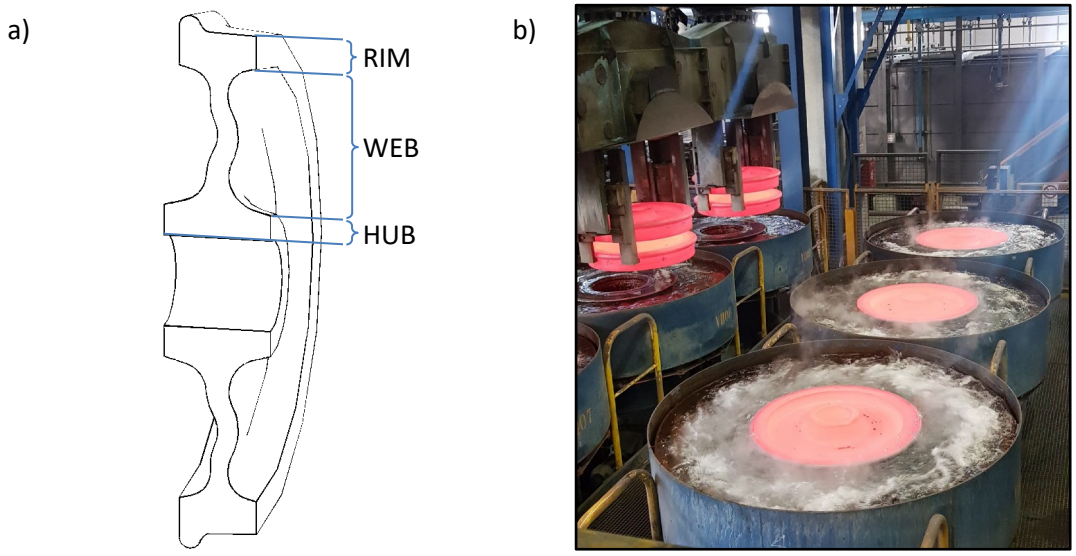

Figure 3: a) Cross section of the rail wheel used in this study (b) Rim chilling facilities at Lucchini RS in Lovere, Italy

3.1.2. Rail steel

Medium and high carbon steels with similar compositions are used for railways globally; however, the designations and preferences can differ between regions. Various rail grades are used throughout Europe. Although the use of heat treated (premium) rail grades are becoming more common, and bainitic variants are being studied, the standard pearlitic R260 rail grade is still widely used throughout Europe. This is also considered the economic choice for straight track and areas where only light RCF and wear is expected [34]. EN 13674 is used to standardise the European rail grades – Table 1 shows the standard chemical composition for the two accepted R260 rail grades [35,36].

Rail design and maintenance

The EN 13674 standard is presented in four parts. Parts 1 and 4 focus on the Vignole rails, with the distinction that Part 1 is for heavier rails (46 kg/m and above) and Part 4 for the lighter rails (from 27 up to 46 kg/m) [35,36]. Vignole rails are symmetrical, flat-bottomed rails and accounts for most rails in service. Most European infrastructure managers use heavier rail profiles – the 54E1 and 60E1 profiles are very common. Figure 4 shows the rail profile 60E1 as specified in EN 13674-1 [35].

The profile of the rail is important, as it influences the wheel-rail interface – improper contact between the wheel and the rail can result in damage on either component and lead to an increased need for maintenance or premature replacement. Rail maintenance strategies should therefore include reprofiling. At the same time, the rail maintenance activities such as grinding or milling, should be

optimised to ensure that no changes occur in the microstructure. EN 13674 requires a fully pearlitic microstructure; improper machining activities can cause thermal damage in the surface layer of the rail, which can result in unwanted microstructures such as martensite.

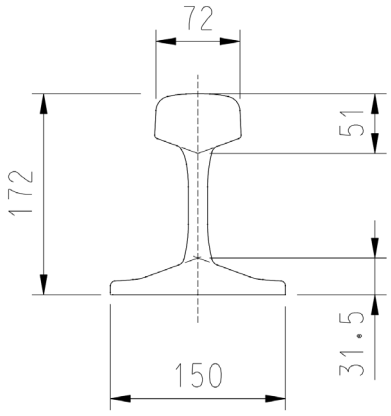

Figure 4: UIC 60E1 Vignole rail profile

3.1.3. Materials considered in this research

The work presented in this licentiate thesis is performed on railway wheel steel ER7T as described in Section 3.1.1. Future work (see Section 6.2) will be performed on rail steel R260 as described in Section 3.1.2. Although there are some compositional differences between these two materials, both have the pearlitic microstructure of interest. The investigation of thermo-mechanical fatigue and material behaviour can benefit both the rail and railway wheel industries. It is beneficial to compare these materials – not only can new research and established principles then be applied to both fields, but these learnings can be used to improve simulations and best-practices on both rails and railway wheels.

3.2 Microstructures of interest

3.2.1 Pearlitic microstructure

Morphology and formation

Pearlite is a common microstructure found in steels where austenite transforms into a two-phase microstructure consisting of ferrite and the carbide cementite (Fe_3C). Eutectoid austenite will form a lamellar pearlitic microstructure – the ferrite and cementite lamellae will grow together from the austenite grain boundaries. This can result in pearlite colonies with different orientation within the original austenitic grain [37].

Lamellar growth occurs by carbon diffusion, which is highly dependent on the available energy. This implies that slow cooling rates allow for carbon to diffuse larger distances, forming coarse pearlite that has larger interlamellar spacing (ISP). Fine pearlite can be formed by increasing the cooling rate, effectively limiting the distance that carbon can diffuse. A pearlitic microstructure can also be obtained

by isothermal decomposition of austenite, where the material is quenched to below the eutectoid temperature (A_{C1}) and held isothermally until the austenite is fully transformed. Lower temperatures result in finer pearlite [37,38].

Railway wheel steel ER7T is a hypoeutectoid steel with 0.52 wt% (max) carbon, where some ferrite forms before the eutectoid reaction occurs. This pro-eutectoid ferrite (or free ferrite) could be considered as a microconstituent of the pearlitic microstructure and is clearly distinguishable (see Figure 5). In the case of isothermal decomposition of austenite, less free ferrite forms than with continuous cooling, which is the explanation to why there is only some 10 vol% free ferrite in the rim-chilled wheel surfaces.

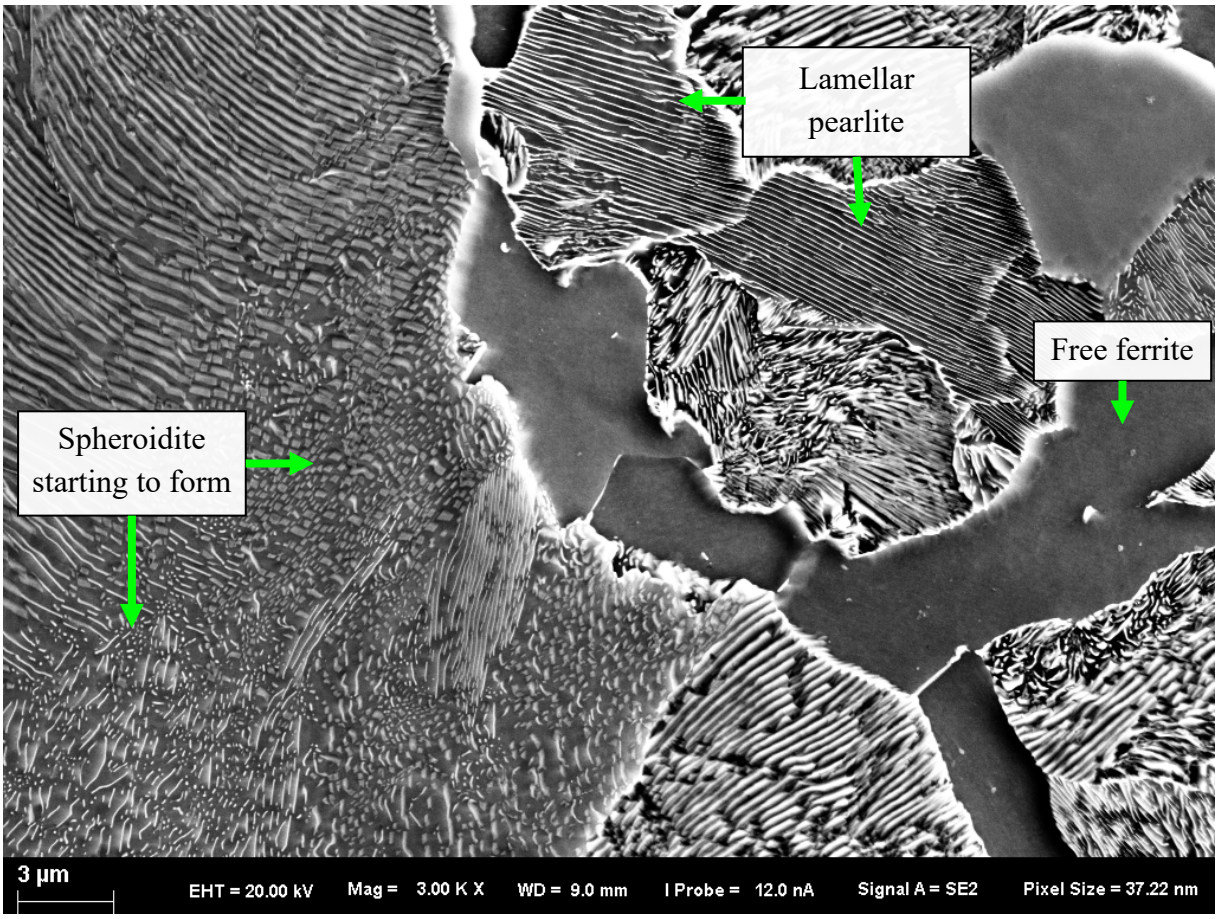

Figure 5: Features in the pearlitic microstructure of railway wheel steel ER7T

Spheroidite

Spheroidite, or spheroidised pearlite, can form when lamellar pearlite is exposed to elevated temperatures, just below the eutectoid transformation temperature (A_{C1}). The surface area of a sphere is the smallest possible per unit volume, so an increase in temperature results in the two-phase microstructure to spheroidise the minor phase, in this case cementite [37]. It has also been shown that the degree of spheroidisation is both time and temperature dependent [22,37–39].

The pearlitic microstructure is idealised as flat and evenly distributed lamellae. In reality the cementite lamellae are often curved and discontinuous, with gaps or holes [40] as shown in Figure 6a and b below. According to the fault migration theory [41], these curved regions or discontinuities have higher chemical potential and can act as initiation sites for spheroidisation. Discontinuities can also be formed by plastic deformation [42]. During spheroidisation, the cementite lamellae break apart into smaller flakes or pieces (see Figure 6c), which coarsens to form spheroids. Although the shape of the lamellae affects the rate of spheroidisation, it is suggested that the interlamellar spacing has a very small effect in this regard [22].

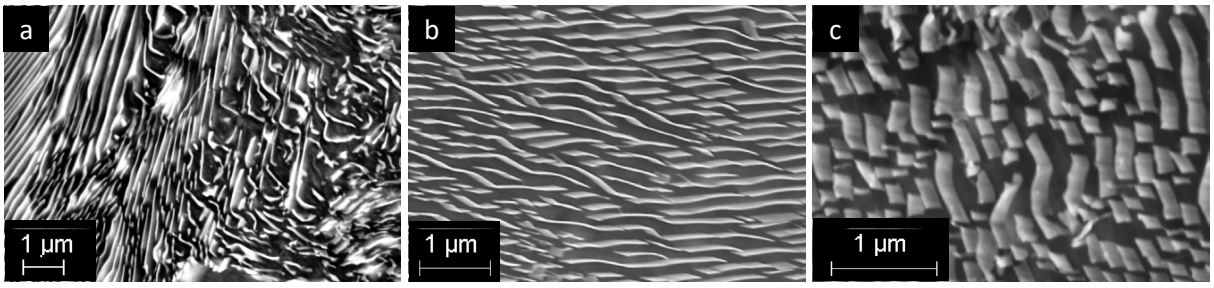

Figure 6: Curved lamellae and discontinuities can act as initiation points for spheroidisation. (a) Irregular shaped pearlitic lamellae (b) Curved pearlitic lamellae with discontinuities (c) Cementite lamellae start to break apart before it coarsens into spheroids

Mechanical properties

The tensile strength of pearlite is highly dependent on the concentration of carbon and manganese. The carbon content dictates the amount of lamellar pearlite that can form, which allows for dispersion strengthening. The addition of manganese can shift the eutectoid composition to lower carbon contents (i.e., increasing the amount of pearlite formed), and it acts as a solid solution strengthener and grain refiner. The strength of pearlite is also affected by the interlamellar spacing – a finer microstructure results in higher strength. This could be attributed to the strain hardenability of pearlite [38,42]. The carbon content should however be optimised for strength as well as ductility and toughness. An increase in carbon, and thus in pearlite volume fraction, results in an increase in the impact transition temperature [38]. In conjunction with the high strain hardenability of pearlite, this can result in brittle fracture. The pearlitic structure also provides multiple crack initiation sites.

The room temperature micro hardness of cementite is about 1000 HV [43,44], while for ferrite it is in the range of 145 HV [45]. The hardness of pearlitic steel is dependent on the carbon content and interlamellar spacing – for the same carbon content, a finer pearlitic structure will have higher hardness. For ER7T, the room temperature hardness of the rim is about 270 HV (refer to the hardness map in Figure 4(a) of **Paper II**).

Spheroidisation of pearlite can result in degradation of the intended mechanical properties. With an increase in spheroidite, the strength and hardness will decrease, as these properties depend on the

loss of lamellar structure. At the same time ductility and toughness will increase with more pronounced spheroidisation.

Dynamic strain ageing

The small amount of interstitial carbon and nitrogen present in iron is responsible for the yield point effect during room temperature tensile testing of iron and by extension, in steel [46]. After the lower yield limit is reached, a horisontal (or flat) region is often observed – this is called the Lüders elongation [47–49] and can be characterised as localised plastic deformation. After this elastoplastic transition, generalised work hardening starts, and the stress-strain curve takes on the characteristic upwards slope. An interruption during the Lüders extension, where the material rests at room temperature for an extended time, can lead to diffusion of the interstitial atoms to dislocation sites. This diffusion process can be expedited by increasing the hold temperature to between 80 °C and 200 °C [46,50]. The diffused interstitials pin the dislocation again, resulting in a new yield point on reloading – this phenomenon is referred to as *strain ageing*. Therefore, it is often referred to as *blue brittleness*, as it coincides with the temperatures at which an oxide with a blue interference colour is formed on the steel surface [46].

An increase in testing temperature leads to an increase in the carbon diffusion rate. The interstitial atom diffusion and deformation occurs simultaneously, resulting in the primary yield point being replaced by multiple localised yield points in the material structure. This phenomenon is known as *dynamic strain ageing* (DSA) and is characterised by a serrated appearance of the stress-strain curve [46,51,52]. Testing under DSA conditions can result in decreased material ductility because of the increased dislocation density and carbide nucleation. For ER7T, DSA occurs between approximately 200 °C and 300 °C (depending on the applied strain conditions).

3.2.2 Martensite

Martensitic transformation is a rapid diffusionless process which can occur in steel when it is quenched from the austenitic phase to room temperature [37,53]. An increase in carbon content lowers the temperature at which martensite starts to form (M_s) – low carbon steel with about 0.2 wt% carbon has an M_s of about 500 °C, while M_s is about 400 °C for 0.5 wt% carbon steel. A similar decrease is seen for the temperature at which the transformation is complete (M_f) – for a steel with 0.5 wt% carbon this is around 150 °C [54]. At higher carbon contents, not all austenite is transformed to martensite. This *retained austenite* should be considered during heat treatment design, as it can transform to martensite or pearlite during subsequent heating cycles. If these transformations aren't controlled, it can cause unwanted dimensional changes and additional residual stresses [53].

During rapid cooling, the carbon remains in solid solution. The austenite forms a body-centered tetragonal (bct) crystal structure to accommodate the carbon atoms. The tetragonality of the structure is higher for higher carbon contents [37,53]. This change in crystal structure results in a volume increase

– for a free body of 0.5 wt% carbon steel, this can be about 5 % [10]. Consequently, in components where only parts transform to martensite, residual stresses are induced in both the martensite (compressive) and the surrounding material (tensile).

Martensite has very high strength and hardness; however, it is very brittle. In railway operations, as discussed in Section 2, such hardened regions can break from the wheel or rail surface – this is called "spalling". To extend the use of martensitic steels, it can be tempered at temperatures below the eutectoid temperature. This *tempered martensite* is a two-phase microstructure of ferrite and dispersed carbide which has improved toughness and somewhat reduced hardness [37].

3.3 Fatigue behaviour

Fatigue can be defined as the gradual change of the material structure when it is subjected to repetitive (or cyclic) loading below the ultimate tensile strength of the material. In most steels this is a permanent localised change that can lead to degradation of the mechanical properties, cracking, and ultimate failure [55,56]. Fatigue behaviour can generally be characterised as either high-cycle fatigue (HCF), low-cycle fatigue (LCF) or thermal fatigue, and materials need to be tailored for the specific operating conditions [55]. Previous studies have investigated the LCF behaviour of railway materials [57–59] – here the load cycling is characterised by a relatively low number of cycles with a substantial amount of plastic deformation. Thermal fatigue is also a common phenomenon in railway operations such as block braking. In this case the cyclic stress is caused by heating and cooling cycles which result in repeated thermal expansion and contraction [55].

Different failure mechanisms can occur simultaneously, resulting in a unique fatigue behaviour. An example of this is thermo-mechanical fatigue (TMF), where mechanical and thermal cycling is combined either in-phase or out-of-phase [60–62]. These combined loadings can result in much higher levels of damage than that experienced during isothermal loading. A further complication is the addition of oxidation or creep which can amplify the damage incurred during thermo-mechanical loadings.

Both railway wheel and rail material experiences thermo-mechanical loading during operation and maintenance. Although this research topic is gaining traction in the railway research community [63,64], the complex nature of the material behaviour and microstructural changes during thermo-mechanical loading needs to be better understood.

RESEARCH METHODOLOGY

4.1 Samples

The work presented in this thesis was done on railway wheel steel ER7T as discussed in Section 3.

In **Papers I and II** the thermo-mechanical behaviour during slow heating and controlled cooling was studied for both the wheel rim and web material of virgin wheels. Cylindrical test bars were supplied by Lucchini RS from the locations as indicated in Figure 7a; Figure 7b gives the dimensions of a typical test bar.

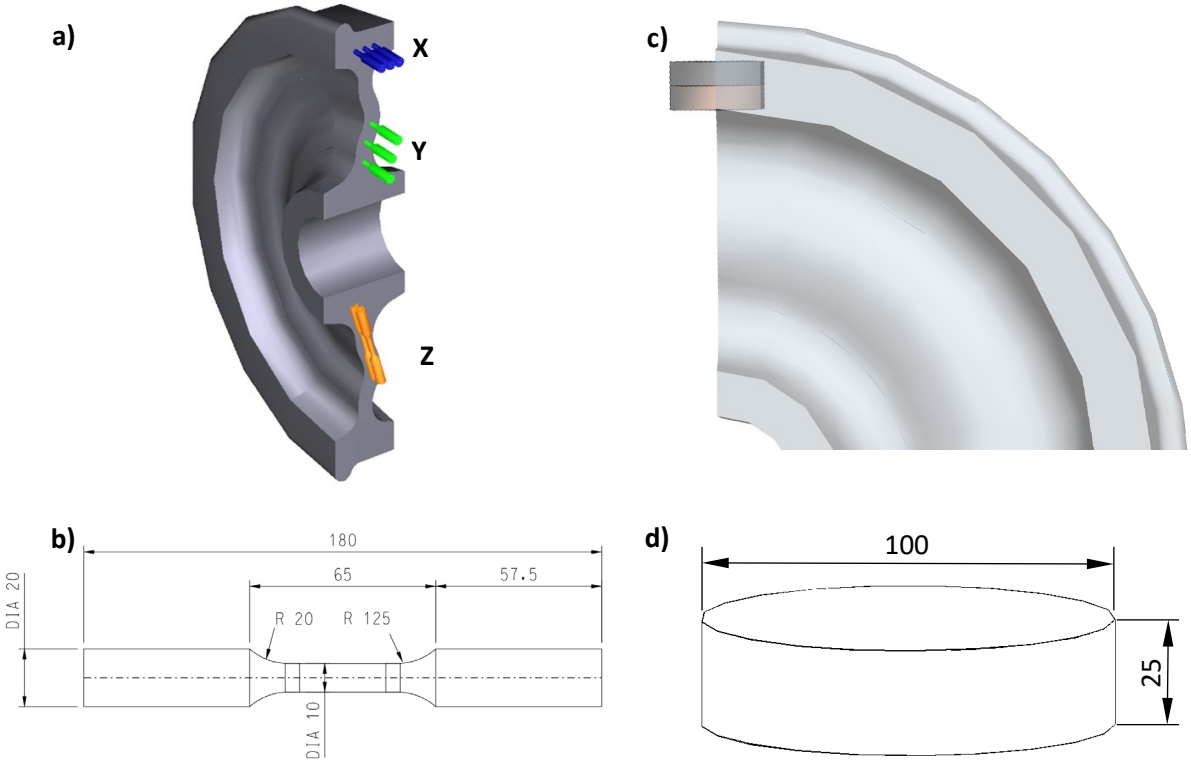

Figure 7: a) TMF sample locations. Distinction is made between rim samples (X), circumferential web samples (Y) and radial web samples (Z). (b) Standard test bar geometry (c) Position where the build plates were taken from the wheel rim. (d) Machined size of each build plate.

The effect of rapid heating and cooling on wheel rim material was studied in **Paper III** using samples taken from the wheel rim (location as shown in Figure 7c) with a diameter of 100 mm and thickness of 25 mm as shown in Figure 7d. An unused ER7T railway wheel was supplied by Lucchini Sweden AB; these samples, or build plates, were machined from the rim to fit an EOS M100 metal printer (see Section 4.3 for more detail). The surface used for the study in **Paper III** is from a depth of approximately 30 mm below the wheel rim surface, at a plane parallel to the surface.

4.2 Thermo-mechanical testing

The study in **Paper II** was aimed at improving existing numerical models to include the thermo-mechanical effects of severe block braking. The thermo-mechanical testing, as described in **Paper I**, was used to calibrate this new numerical model.

4.2.1. Test setup

Thermo-mechanical testing was done using induction heating on an MTS 809 servo-hydraulic biaxial test frame fitted with a 100 kN load cell. K-type thermocouples were welded onto the test bar in two places – one for control in the centre of the gauge section and the other as a safety measure on the radius of the lower grip section. The thermocouples were spot welded around at least half the circumference of the test bar. An MTS water-cooled high-temperature extensometer fitted with ceramic extension rods were used to measure the strain. Figure 8 shows a photo of the setup.

Figure 8: Experimental setup

4.2.2. Procedure

The strain-controlled thermomechanical testing was done according to the TMF code-of-practice [65]. The testing procedure, as outlined in Figure 9, is described below.

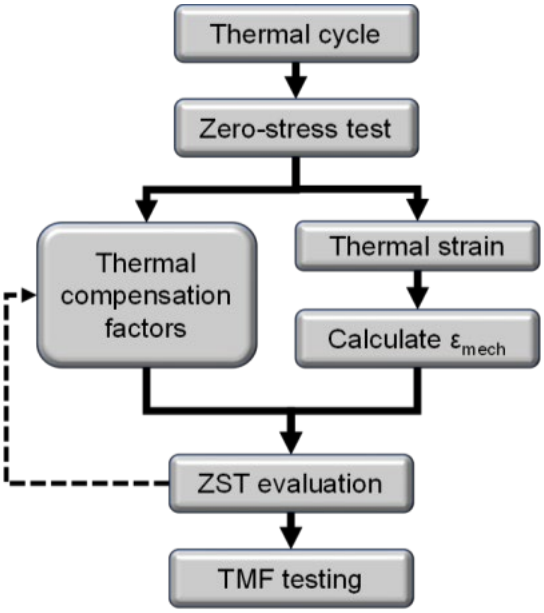

Figure 9: Outline of the procedure used for TMF testing

Application and thermal cycle

The numerical model developed in **Paper II** used a thermal cycle with a peak temperature of 650 °C as the initial case, based on field study measurements and previous models for tread braking [66–69]. However, this would allow for the worst-case scenario. Typically, the rim material would seldomly be exposed to peak temperatures above 600 °C, while the peak for the web material is expected to be 300 °C at maximum.

To allow for the scaling of the initial thermal cycle to other peak temperatures, two exponential functions were used to describe the heating and cooling curves respectively:

$$T_H = -700ke^{-0{,}00098x} + 700k$$
$$T_C = 3300ke^{-0{,}00056x} - 40k$$

with T_H the temperatures on the heating curve, T_C the temperatures for the cooling curve, x the time (in seconds) and the scaling factor, k, a factor relative to 650 °C, i.e.:

$$k = \frac{T_2}{650}$$

Initial testing of the rim samples was done with a baseline, or minimum, temperature of 30 °C. However, due to fluctuations in ambient conditions and instability of the induction heating at such low temperatures, this was increased to 50 °C. The simulated braking cycle was 45 minutes long; therefore, the duration of the heating cycle was kept constant at 45 minutes for all peak temperatures. The cooling

cycle was approximately 60 minutes, with slight variations to allow for the material to reach the baseline temperature while following the same cooling rates.

Zero-stress test

The testing procedure starts with a zero-stress test (ZST), where the sample is subjected to the programmed thermal cycle while free expansion is allowed. During this test, the amount of thermal expansion, i.e., the thermal strain, is measured. Five thermal cycles are executed to allow for stabilisation of the material, after which another five evaluation cycles are recorded to use for subsequent calculations.

Thermal compensation and calibration

Typically, the measured strain in a constant temperature test is the total strain as detected by the extensometer. In a TMF test, thermal expansion of the gauge section must be subtracted from the measured total strain to achieve the mechanical strain. During the zero-stress test, the measured total strain would then be equal to the thermal strain. When mechanical strain (induced by force application) is applied, the total strain becomes the sum of the mechanical and thermal strains.

In this study, mechanical strain and temperature variation was defined, and strain-controlled testing was done. To evaluate the mechanical strain separately, the thermal strain needs to be removed from the total measured strain through thermal compensation (see Figure 10). The thermal strain measured during the zero-stress test is used to calculate thermal compensation factors. Thermal compensation is a programmed function of the MTS testing software where the thermal strain is calculated, then subtracted from the total measured strain. The thermal strain is calculated at every time from the temperature measured at the centre of the gauge section using the following formula:

$$\varepsilon_{th} = \boldsymbol{E_2}T^2 + \boldsymbol{E_1}T + \boldsymbol{E_0}$$

Sufficient compensation factors E_2, E_1 and E_0 should be found through an iterative process – by adjusting these factors, the calculated thermal strain can be fitted to the measured thermal strain from the zero-stress test. The closer the fit, the better the thermal compensation (i.e., the removal of the thermal strain from the final total strain) will be. Following the guidelines of the TMF code-of-practice [65], thermal compensation was considered sufficient if the following criteria were met during the evaluation run:

- Peak stress values should be lower than 0.05 x Δσ (full stress range of the TMF test)
- Mean stress should be lower than 0.02 x Δσ (full stress range of the TMF test)

Determining strain values and TMF testing

As discussed in **Paper II**, the simulated use-case accounted for mechanical strains between 30 % and 60 % of the thermal strain at different positions in the wheel. The applied mechanical strains (now the

total measured strain after compensation) should therefore be calculated as percentages of the measured thermal strains.

To cover the entire spectrum, five degrees of thermal dilatation restriction were investigated in this study:

a. Free expansion. Mechanical strain, and thus the degree of thermal dilatation restriction, is zero.
b. 25 % thermal dilatation restriction
c. 50 % thermal dilatation restriction
d. 75 % thermal dilatation restriction
e. Full restriction. Mechanical strain is equal to 100 % the calculated thermal strain, and thermal dilatation is fully restricted.

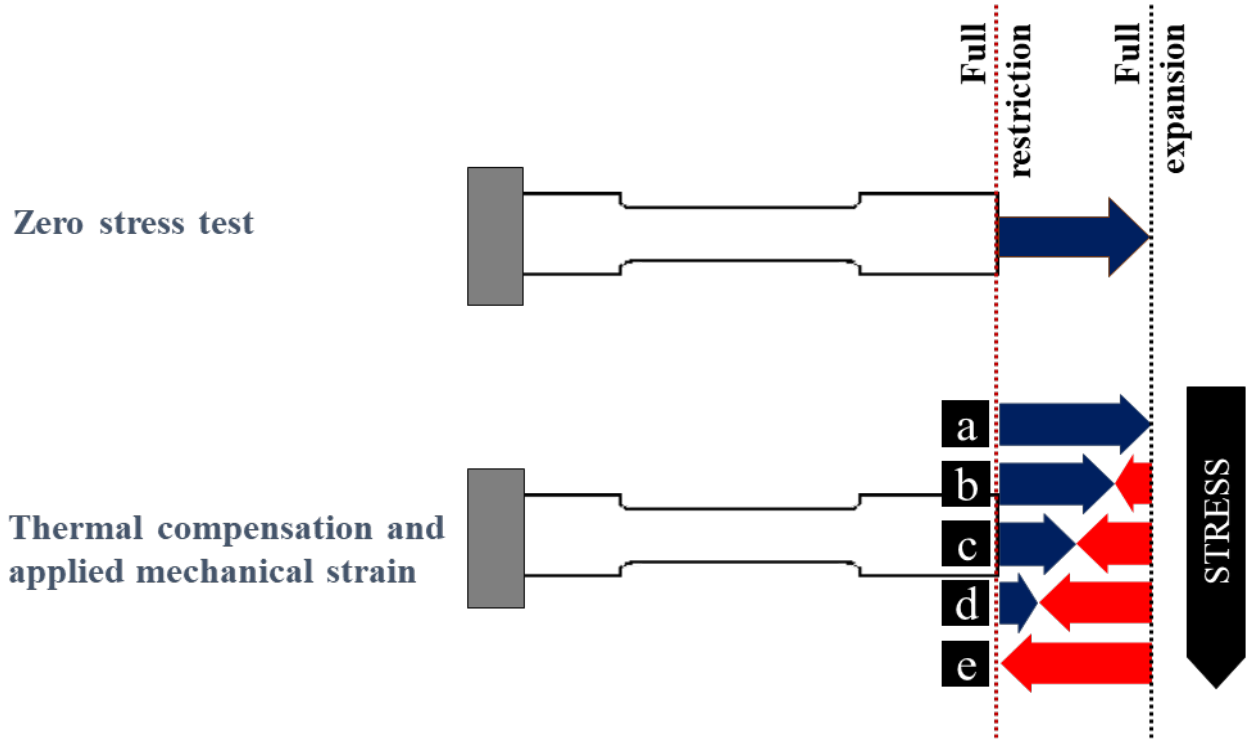

Figure 10: Thermal compensation and strain application during thermo-mechanical testing.

Figure 10 is a visual representation of the process. During the zero-stress test (ZST), full expansion is allowed; the machine controller is set to maintain zero axial force and the strain measured is thus only due to thermal expansion. Thermal compensation is then tuned to remove the effect of thermal expansion (i.e., thermal strain). With thermal strain removed by the software, the total strain is equal to the applied mechanical strain:

$$\varepsilon_{total} = \cancel{\varepsilon_{thermal}} + \varepsilon_{mechanical}$$

To get a zero-stress case (full expansion) even if we run the test under strain control, we need to counter-act the thermal compensation by applying a mechanical strain. As an example, case **a** in Figure 10 shows how free expansion is simulated by applying mechanical strain equal to 100 % of the thermal strain as measured during the ZST. In essence, this is a test of how well the thermal compensation works, and the smaller the stress levels registered the better. Cases **b** to **d** show different degrees of restriction of the thermal dilatation and case **e** shows full restriction where the total strain is set to zero. Five thermal cycles were performed for each strain case at each peak temperature. Four test series were conducted on the wheel rim material at peak temperatures of 300, 400, 600 and 650 °C respectively. Test series were also completed for both the circumferential and radial web samples (as described in Section 4.1) at a peak temperature of 300 °C, and for the circumferential web samples at 650 °C.

4.3 Laser scanning

In **Paper III** the effects of rapid heating and cooling on near pearlitic railway wheel steel is investigated. This is done through comparing the results of laser scanning using the laser sources in two types of equipment: laser-based powder bed fusion (LB-PBF) additive manufacturing equipment and laser welding equipment. An overview of the experiments is given below.

4.3.1 Weld simulation using LB-PBF equipment

The LB-PBF additive manufacturing (AM) technique uses focused laser to fuse material powder to build up a component [70]. For this experiment, no powder was added; instead, the effect of the laser scanning only heating the bulk material was investigated. The aim of this experiment was to simulate the conditions in the heat affected zone of a repair weld.

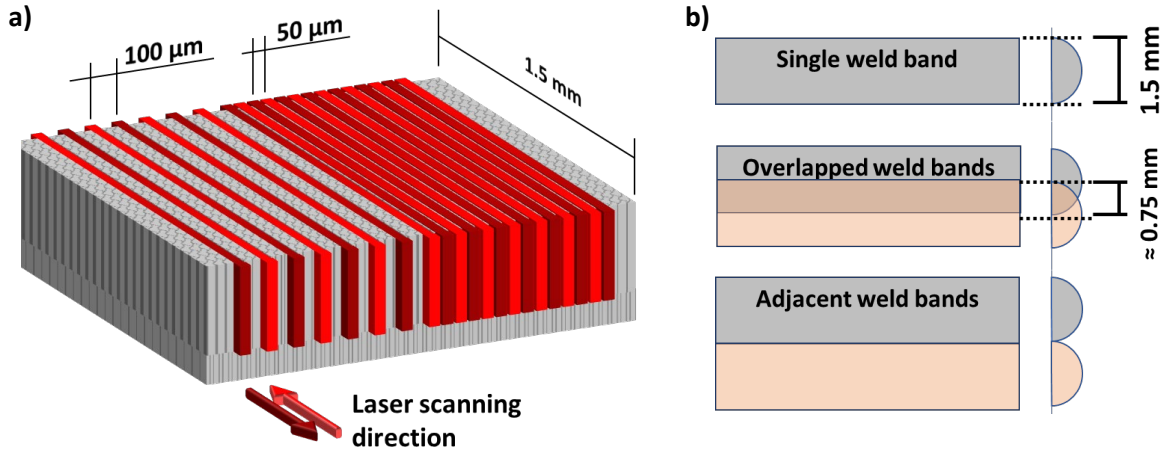

Figure 11: a) Close-up illustration of the laser scanning showing the hatch distance between laser scans in alternating directions (b) Scenarios to investigate the effect of subsequent scans

The laser speed and power density distribution can be varied depending on the requirements of the experiment: the melt pool size and stability is dependent on the laser scan speed, whilst the power

density distribution affects the material temperature [70,71]. For the experiment discussed in **Paper III**, an effective laser power of 170 W and beam diameter of 40 μm was used. A zig-zag pattern was used to simulate a weld band with a width of 1.5 mm. Two different hatch spacings (50 μm and 100 μm) were considered, as shown in Figure 11a, as well as two different scan lengths (1.5 mm and 15 mm). To evaluate the tempering capacity of subsequent scans, three scenarios were compared (see Figure 11b).

4.3.2 Weld simulation using laser welding equipment

Heating by scanning with laser welding equipment was compared with the LB-PBF scans to understand how the variation in heat input from different process parameters can affect the material properties. The laser welder scanning was done on the same build plate as used for the AM scans to ensure the same initial condition. In the experiment as discussed in **Paper III**, the scan speed and applied power was varied and the resulting microstructural changes due to variation in heat input was investigated. The tempering capacity of subsequent scans was considered as for the AM scanning.

4.4 Heat treatment

Previous studies on pearlitic railway wheel steel have shown that variation in mechanical properties, specifically room temperature hardness, can be expected after exposure to temperatures exceeding 500 °C [10,12,18]. To confirm that the hardness variation observed after TMF experiments was a result of the combined thermal and mechanical loads rather than the elevated temperature alone, heat treatment was performed on virgin ER7T samples. A ceramic tube furnace with an argon atmosphere was used for the heat treatments and samples were allowed to air-cool. The following heat treatment was done on both rim and web samples (12 samples in total):

- 200 °C for four hours
- 250 °C for four hours
- 300 °C for 30 minutes and four hours (one sample each)
- 350 °C for 30 minutes and four hours (one sample each)

4.5 Hardness

Mounted samples were prepared by mechanical polishing down to 1 μm with diamond solution and finally active oxide (colloidal silica) polishing to 0.04 μm. Room temperature hardness testing was done using a Struers DuraScan-70 G5 hardness tester made by Emcotest. The hardness of virgin and TMF tested samples, as discussed in **Papers I** and **II**, was evaluated. At least five random Vickers hardness (HV) indentations were made on each sample with a load of 30 kg and a hold time of 12 seconds.

Additionally, a hardness map of the wheel profile was created for **Paper II**, using the same parameters.

To characterise the microstructural changes during rapid heating and cooling as discussed in **Paper III**, Vickers hardness (HV) indents were made with a load of 1 kg and a hold time of 12 seconds across the top surface of each weld band (as discussed in Section 4.3).

4.6 Microscopy

Stereo optical microscopy was used for the surface evaluation of the scanned regions in **Paper III**. A Zeiss Stereo Discovery V20 microscope with AxioVision V.4.7 software was used for this analysis. Electric discharge machining (EDM) was used to cut a 5 mm slice from the build plate surface (see Figure 12) to create cross-sections of the different scanned regions (as described in Section 4.3).

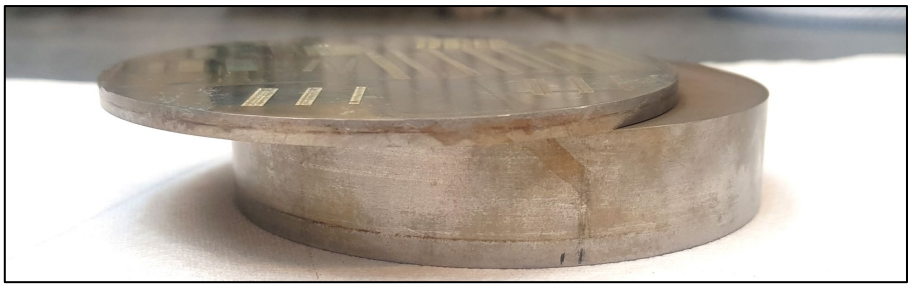

Figure 12: slice cut from build plate surface to prepare samples for microscopy

The same metallographic preparation procedure was used as for the TMF samples and etching was done with 3 % nital (HNO_3 in ethanol) for 15 to 20 seconds. The microstructure of the cross-sectional samples for **Paper III** was investigated using a Zeiss Axioscope 7 light optical microscope with Zen Core 2.7 software. The microstructural analysis and subsequent spheroidisation quantification for **Papers I** and **II** required a higher magnification. Therefore, scanning electron microscopy was done using both a LEO Gemini 450 and a LEO Gemini 1550 field emission gun scanning electron microscope (FEGSEM). For the quantification of cementite spheroidisation, at least 20 high contrast images were taken at random locations for each sample at a magnification factor of 5 000.

4.7 Residual stress measurements

Residual stress measurements were done for the study presented in **Paper III** using a Stresstech Xstress 3000 X-ray diffractometer with a type G2R tripod-mounted goniometer and a Cr Kα X-ray source. A 1 mm collimator was used to focus the X-rays and calibration was done on pure ferrite (Fe). Residual stress was measured on the top surface of each of the laser scans at inclination angles varying from -45° to 45° (in nine equal steps), each at three different rotation angles (0°, 45° and 90°). A Split Pearson VII fit was applied to the intensity distribution measures and the principal stresses were evaluated.

ANALYSES AND RESULTS

This chapter provides a brief summary of the analyses and results obtained from the individual studies as presented in **Papers I to III**.

5.1 Thermo-mechanical behaviour of railway wheel steel

To better understand the complex interaction of mechanical and thermal loads, a use case for severe block braking was simulated. **Paper I** investigates the stress response of railway wheel steel ER7T under combined thermal and mechanical loading. Peak temperatures of 300, 400, 600 and 650 °C are investigated and the thermal dilatation (expansion) is restricted to different degrees. As the degree of thermal dilatation restriction is increased (for a given peak temperature), the peak stress increases, and increasing levels of plasticity is visible. Similarly, as the peak temperature is increased, the resulting stress after cooling increases for the same degree of thermal dilatation restriction. However, this increase in stress is counteracted by changes in the microstructure – as the peak temperatures increase, and increase in spheroidised pearlite is noted, accompanied by a reduction in room temperature hardness.

In **Papers I and II** it was suspected that variation in mechanical properties, such as hardness, occurs at lower temperatures for thermo-mechanical testing than for isothermal fatigue testing [18]. Figure 13 shows that a decrease in hardness occurs at peak temperatures exceeding 600 °C as expected from isothermal test results. However, slight variations can be observed in the room temperature hardness for the tests with lower peak temperatures.

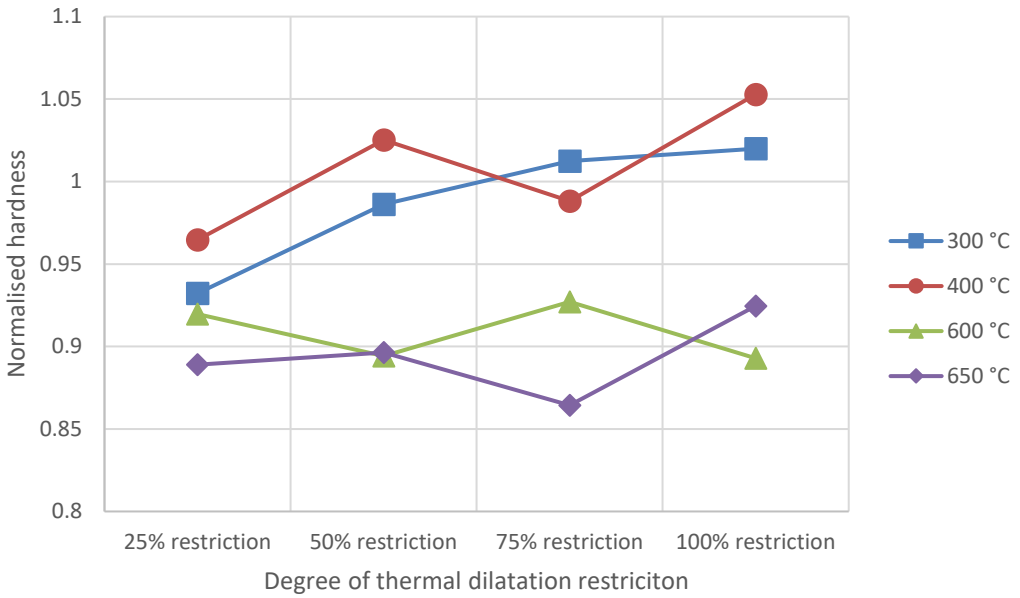

Figure 13: Variation in normalised room temperature hardness for wheel rim samples exposed to different peak temperatures and degrees of thermal dilatation restriction

Heat treatment experiments (see Section 4.4) were performed to prove that this variation is in fact due to the combined mechanical and thermal loads, rather than a result of the heat treatment alone. Table 2 shows the room temperature hardness of the virgin samples as reference as well as the hardness results for the different heat treatment experiments (not included in appended papers). This shows that temperature alone, at peak temperatures below 400 °C, does not affect the hardness of the material.

Table 2: Room temperature hardness of heat-treated samples

	Room temperature hardness (HV)			
	Rim material		Web material	
Virgin sample (minimum, maximum)	278	286	189	198
Heat treatment	30 minutes	4 hours	30 minutes	4 hours
200 °C	-	282	-	198
250 °C	-	281	-	198
300 °C	282.5	282	194	193
350 °C	287	282	193	192

In **Paper II** the experimental data from the TMF tests are used to calibrate a new constitutive material model for severe block braking. It captures the thermo-mechanical behaviour better than previous models, but there are still further experiments and model developments to include all aspects of the complex thermo-mechanical behaviour.

5.2 Effect of rapid heating and cooling on residual stress state

To contrast the slow heating and cooling cycles as investigated for **Papers I and II**, the effects of rapid heating and cooling was investigated in **Paper III**. The intent of this study is to form a basis for subsequent studies into rapid, local heating events such as rail repair welding or grinding. The resulting residual stress state was evaluated after laser scanning using additive manufacturing equipment and laser welding equipment (see Section 4.3).

Figure 14 shows a comparison of these residual stresses - Table 3 shows the scan parameters for each of the represented scans. The as-machined stress (leftmost values) shows the principal residual stress for the build plate as received. As expected, stress relieving resulted in a very low residual stress state – these values are used as reference values for the subsequent laser heating experiments. **Paper III** investigates why these variations in residual stress occurs and how this can help to relate different laser heating techniques.

Table 3: Clarification of scan parameters for Figure 14

AM laser scanning				
Scan ID	**Scan format**	**Hatch spacing**	**Scan length**	**Scan speed**
AM-1a	Single scan	50 µm	1.5 mm	5.3 mm/s
AM-2a	Single scan	100 µm	1.5 mm	
AM-3a	Overlapped scans	50 µm	15 mm	
AM-3b	Overlapped scans	100 µm	15 mm	
Laser weld scanning				
Scan ID	**Scan format**	**Pulse frequency**	**Pulse duration**	**Scan speed**
LW-1a	Single scan	150 Hz	2 ms	5.3 mm/s
LW-2a	Single scan	150 Hz	1 ms	1.3 mm/s
LW-2b	Single scan	150 Hz	2 ms	1.3 mm/s
LW-3a	Single scan	100 Hz	2 ms	6.3 mm/s

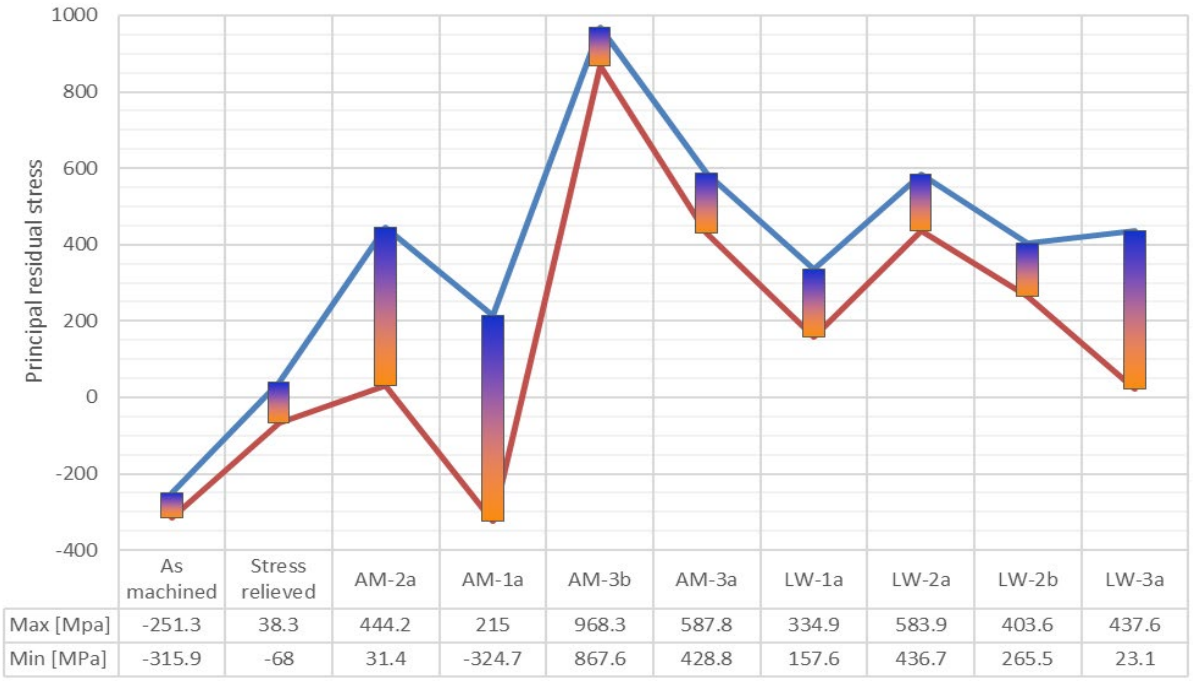

Figure 14: Comparison of residual stresses after heating with different laser scanning techniques

5.3 Microstructural analyses

In **Paper I** the spheroidisation of pearlite is investigated during slow heating and cooling. Figure 15 shows a comparison of the amount that the railway wheel material is spheroidised when exposed to different peak temperatures. In this paper it is shown that an increase in peak temperature results in a higher degree of cementite spheroidisation, similar to what is seen in isothermal testing. During rapid heating above the austenitisation temperature and subsequent rapid and cooling, as investigated in **Paper III**, martensite can form. This is observed during heating by laser scanning using both additive manufacturing and laser welding equipment – two examples are shown in Figure 16.

Both spheroidisation and martensite formation can result in diminished mechanical properties and material performance in operation. These studies help to form an understanding of these phenomena and how local heating processes can be tailored to minimise the detrimental effects of such microstructures.

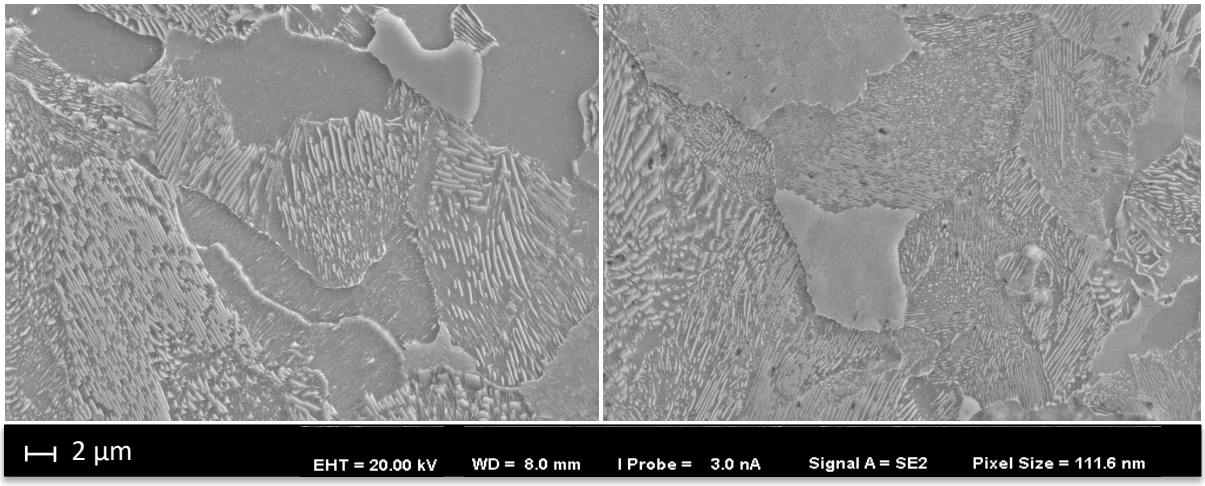

Figure 15: SEM micrographs of samples that were exposed to 75 % thermal dilatation restriction and peak temperatures of 300 °C (left) and 650 °C (right) respectively.

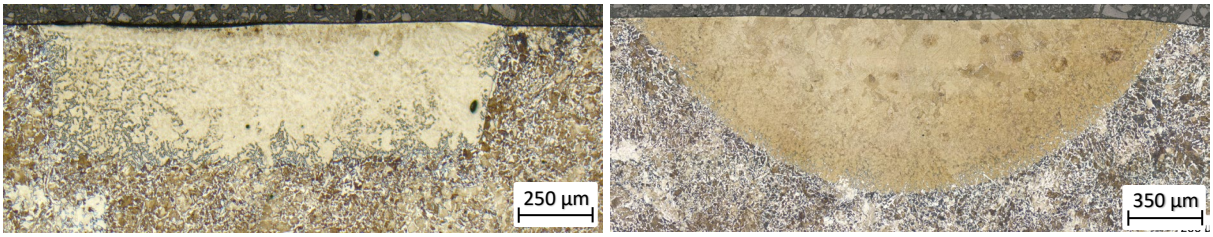

Figure 16: Optical microscopy images of the transformed microstructure region created by laser scanning using additive manufacturing equipment (left, see scan AM-2a in Table 3) and laser welding equipment (right, see scan LW-2d in Table 3).

CONCLUDING REMARKS

6.1 Research objectives as addressed in appended papers

This thesis work investigates the thermo-mechanical behaviour of railway wheel steel (ER7T) during high temperature processes.

- **Paper I** provides insight into the material behaviour of this ferritic-pearlitic railway wheel steel during severe block braking (i.e., slow heating and cooling). It is shown that both thermal cycling and the degree of thermal dilatation restriction affects the mechanical properties and material structure.
- **Paper II** details how the experimental data is used to validate a new numerical model for severe block braking. This study underlines the complexity of the thermo-mechanical behaviour, and it is seen that numerous model parameters are introduced to compensate for the actual behaviour.
- **Paper III** investigates the effect of rapid heating and cooling events on the microstructure and residual stress state of the railway wheel steel. This study provides insight into the similarities and differences of different rapid heating (high temperature) processes – this can be used to support the development of more accurate welding simulations.

6.2 Future work

This licentiate thesis work forms part of the doctoral thesis project to improve understanding of high temperature processes on both rail and railway wheel steel. The continuation of this work can be divided into three focus areas:

- Concluding the investigation into the thermo-mechanical behaviour of railway wheel steel ER7T.

  The investigations to date have provided insight into the material behaviour on a global level. An ongoing study will provide a better understanding of the residual stresses at grain level, which can be used to explain the global residual stress and to better understand the phenomena seen on a global scale. This work has been presented at the 2022 TMS conference [72] and is now being written up for publication.

- Investigating the thermo-mechanical behaviour of rail steel R260

  This will be the major focus for the remainder of the research project. Some specific focus points include:

- Simulating rail repair welding conditions in controlled experiments to improve the thermo-mechanical behaviour of rail steel during rapid heating and cooling processes. This will also be used in calibration studies for the simulation of these high temperature processes.
- Investigating transformation plasticity to identify the material behaviour and provide data for improved simulations.
- Investigating martensite formation during high temperature processes to improve microstructural characterisation and to provide data for improved simulations.

- Comparing the behaviour of railway wheel steel ER7T and rail steel R260 to support future studies into the thermo-mechanical behaviour of rail steel.

  The material behaviour of these materials will be compared for both slow heating and cooling rates (as for **Paper I**) and for rapid heating and cooling (as for **Paper III**). The same experiments will be repeated for rail steel R260 to compare the mechanical properties and degree of spheroidisation. The intended outcome of this investigation is to determine the comparability of the rail and railway wheel materials, and to support the interchangeability of research findings.

Acknowledgements

Firstly, I want to acknowledge the CHARMEC research group and our industrial partners for the financial support and invaluable practical perspective. I would specifically like to thank Voestalpine, Lucchini Sweden AB and Lucchini RS (especially Andrea Ghidini), for supplying the material used for testing.

Professor Johan Ahlström: I couldn't have hoped for a better supervisor. Thank you for always being available and willing to help. More importantly, thank you for your kindness and encouragement – you help to make this journey possible! I am grateful to my collaborators for pleasant and fruitful discussions; particularly my co-supervisor Professor Magnus Ekh, Professor Lennart Josefson, Björn Andersson, Professor Tore Vernersson and Eric Landström. Also, thanks to Professor Anders Ekberg and Dr. Björn Paulsson: I owe in large part my interest in this field to you!

A special thanks to William Hearn, Sri Bala Aditya Malladi and Dr. Zhuoer Chen from the Centre for Additive Manufacture – Metal (CAM2), as well as Ove Wahlbeck at Alpha Laser GmbH for their insights and assistance with the laser scanning experiments. I'm also grateful to Dr. Eric Tam, Prof. Christer Persson, Dr. Fang Liu and Roger Sagdahl for invaluable advice and guidance along the way. A special mention to Arda Baytaroglu, an Amanuensis Master student, who was always willing to do more even after weeks of sample preparation.

On a more personal note, thank you to my colleagues and friends (both past and present) at the Department of Industrial and Materials Science for good fika discussions and fun hallway banter. To my "Swedish family": Bala, Bharat, Zhuoer, Fiona, Fredrik, Ismail, Marcos and Alberto, life would be dull without you. A special thank you to my parents, Ertjies and Joan, for being my soundboards, proof-readers and personal draughting service when my CAD skills let me down. Finally, thank you to my South African family and friends for the love, support, and prayers – I love you to the moon and back!

Gothenburg, October 2022
Erika Steyn

References

[1] Council of the EU, Press release: Council adopts European climate law, Brussels, 2021. www.consilium.europa.eu/press.

[2] Directorate-General for Mobility and Transport, New transport proposals target greater efficiency and more sustainable travel, European Commission News. (2021).

[3] European Commission, EU transport in figures - statistical pocketbook, 2021.

[4] Directorate-General for Transport and Mobility. Unit C4 - Rail Safety and Interoperability, Europe's Rail Joint Undertaking - Master Plan (draft), Brussels, 2021.

[5] A. Skyttebol, Continuous Welded Railway Rails: Residual Stress Analyses, Fatigue Assessments and Experiments, Doctoral thesis, Chalmers University of Technology, 2004.

[6] B.L. Josefson, R. Bisschop, M. Messaadi, J. Hantusch, Residual stresses in thermite welded rails: significance of additional forging, Welding in the World. 64 (2020) 1195–1212. https://doi.org/10.1007/s40194-020-00912-4.

[7] The European Union horizon 2020 program, WRIST – Innovative Welding Processes for New Rail Infrastructures, Grant Agreement 636164. (2015). https://cordis.europa.eu/project/id/636164/results (accessed August 16, 2022).

[8] Simon Niederhauser, Laser cladded steel – microstructures and mechanical properties of relevance for railway applications, Doctoral thesis, Chalmers University of Technology, 2005.

[9] The European Union horizon 2020 program, INFRASTAR - Innovation and Networking for Fatigue and Reliability Analysis of Structures - Training for Assessment of Risk, Grant Agreement 676139. (2020).

[10] J. Ahlström, Thermal and Mechanical Behaviour of Railway Wheel Steel, Doctor of Philosophy, Chalmers University of Technology, 2001.

[11] J. Jergéus, Railway Wheel Flats. Martensite Formation, Residual Stresses, and Crack Propagation, Doctoral thesis, Chalmers University of Technology, 1998.

[12] K. Cvetkovski, Influence of thermal loading on mechanical properties of railway wheel steels, Doctoral thesis, Chalmers University of Technology, 2012.

[13] C. Jessop, Damage and defects in railway materials: influence of mechanical and thermal damage on crack initiation and propagation, Doctoral thesis, Chalmers University of Technology, 2019.

[14] J. Ahlström, Modelling of properties and damage in wheel and rail materials (CHARMEC MU30), n.d. https://www.chalmers.se/en/projects/Pages/Modelling-of-properties-and-damage-in-wheel-and-rail-materials.aspx (accessed August 16, 2022).

[15] B. Andersson, Modeling of phase transformations and cyclic plasticity in pearlitic steels, Licentiate thesis, Chalmers University of Technology, 2021.

[16] E. Andersson, M. Berg, S. Stichel, Rail vehicle dynamics, KTH, Stockholm, 2007.

[17] M. Fesharaki, T.-L. Wang, The Effect of Rail Defects on Track Impact Factors, Civil Engineering Journal. 2 (2016) 458–473. https://doi.org/10.28991/cej-2016-00000049.

[18] D. Nikas, Influence of combined thermal and mechanical loadings on pearlitic steel microstructure in railway wheels and rails, Doctoral thesis, Chalmers University of Technology, 2018.

[19] R. Lewis, U. Olofsson, eds., Wheel—rail interface handbook, 1st ed., Woodhead Publishing Limited, Cambridge, 2009. https://doi.org/10.1533/9781845696788.

[20] F.E. Kennedy, Thermal and thermomechanical effects in dry sliding, Wear. 100 (1984) 453–476. https://doi.org/10.1016/0043-1648(84)90026-7.

[21] J.R. Barber, The conduction of heat from sliding solids, Int J Heat Mass Transf. 13 (1970) 857–869. https://doi.org/10.1016/0017-9310(70)90131-6.

[22] S. Chattopadhyay, C.M. Sellars, Kinetics of pearlite spheroidisation during static annealing and during hot deformation, Acta Metallurgica. 30 (1982) 157–170. https://doi.org/10.1016/0001-6160(82)90055-4.

[23] R. Andersson, J. Ahlström, E. Kabo, F. Larsson, A. Ekberg, Numerical investigation of crack initiation in rails and wheels affected by martensite spots, Int J Fatigue. 114 (2018) 238–251. https://doi.org/10.1016/j.ijfatigue.2018.05.023.

[24] R. Enblom, Deterioration mechanisms in the wheel–rail interface with focus on wear prediction: a literature review, Vehicle System Dynamics. 47 (2009) 661–700. https://doi.org/10.1080/00423110802331559.

[25] B.-C. Goo, J.-W. Seo, Y.-J. Lee, Effect of Welding Polarity on Mechanical Properties of Submerged Arc Welded Railway Vehicle Wheels, Metals (Basel). 12 (2022) 1381. https://doi.org/doi.org/10.3390/met12081381.

[26] AURORA Project, Remanufacture of rail wheels, Technical Journal: Network Rail Insight. (2022). https://www.twi-global.com/media-and-events/insights/aurora-project-remanufacture-of-rail-wheels (accessed August 24, 2022).

[27] B.-C. Coo, Y.-J. Lee, Railway Vehicle Wheel Restoration by Submerged Arc Welding and Its Characterization, Sci. 2 (2020) 33. https://doi.org/10.3390/sci2020033.

[28] CEN, EN 13262: Railway applications - Wheelsets and bogies - Wheels - Product requirements, Brussels, 2020. www.sis.se.

[29] M. Diener, A. Ghidini, Materials for heavy haul solid wheels: New experiences, in: Proc Inst Mech Eng F J Rail Rapid Transit, 2010: pp. 421–428. https://doi.org/10.1243/09544097JRRT356.

[30] K. Mädler, M. Bannasch, Materials used for Wheels on Rolling Stock, Brandenburg-Kirchmöser, Germany, n.d.

[31] R. Arnaiz Merino, Development of Railway Wheels with Alternative Materials and Production Processes, Master thesis, Graz University of Technology, 2015.

[32] D. Nikas, J. Ahlström, A. Malakizadi, Mechanical properties and fatigue behaviour of railway wheel steels as influenced by mechanical and thermal loadings, Wear. 366–367 (2016) 407–415. https://doi.org/10.1016/j.wear.2016.04.009.

[33] Y. Okagata, Design Technologies for Railway Wheels and Future Prospects, Nippon Steel & Sumitomo Metal Technical Report. 105 (2013).

[34] P. Pointner, A. Joerg, J. Jaiswal, INNOTRACK D4.1.5GL: Definitive guidelines on the use of different rail grades, 2006.

[35] CEN, EN 13674-1: Railway applications - Track - Rail - Part 1: Vignole railway rails 46 kg/m and above, European Committee for Standardization, Brussels, 2017. www.sis.se.

[36] CEN, EN 13674-4: Railway applications – Track – Rail – Part 4: Vignole railway rails from 27 kg/m to, but excluding 46 kg/m, European Committee for Standardization, Brussels, 2019. www.sis.se.

[37] L.H. van Vlack, Elements of Materials Science and Engineering, 6th ed., Addison-Wesley Publishing Company, Ann Arbor, Michigan, 1989.

[38] H. Bhadeshia, R. Honeycombe, Iron-Carbon Equilibrium and Plain Carbon Steels, in: Steels: Microstructure and Properties, Elsevier, 2017: pp. 59–100. https://doi.org/10.1016/B978-0-08-100270-4.00003-2.

[39] N. Nutal, C.J. Gommes, S. Blacher, P. Pouteau, J.P. Pirard, F. Boschini, K. Traina, R. Cloots, Image analysis of pearlite spheroidization based on the morphological characterization of cementite particles, Image Analysis and Stereology. 29 (2010) 91–98. https://doi.org/10.5566/ias.v29.p91-98.

[40] M.-X. Zhang, P.M. Kelly, The morphology and formation mechanism of pearlite in steels, Mater Charact. 60 (2009) 545–554. https://doi.org/10.1016/j.matchar.2009.01.001.

[41] Y.L. Tian, R.W. Kraft, Mechanisms of Pearlite Spheroidization, Metallurgical Transactions A. 18 (1987) 1403–1414. https://doi.org/10.1007/BF02646654.

[42] M. Umemoto, Y. Todaka, K. Tsuchiya, Mechanical properties of cementite and fabrication of artificial pearlite, 2003.

[43] M. Umemoto, Z.G. Liu, H. Takaoka, M. Sawakami, K. Tsuchiya, K. Masuyama, Production of bulk cementite and its characterization, Metallurgical and Materials Transactions A. 32 (2001) 2127–2131. https://doi.org/10.1007/s11661-001-0024-y.

[44] H.K.D.H. Bhadeshia, Cementite, International Materials Reviews. 65 (2020) 1–27. https://doi.org/10.1080/09506608.2018.1560984.

[45] E. Duka, H. Oettel, T. Dilo, Connection between micro and macro hardness pearlitic-ferritic steel, in: 2012: pp. 47–51. https://doi.org/10.1063/1.4751563.

[46] H. Bhadeshia, R. Honeycombe, Strengthening of Iron and Its Alloys, in: Steels: Microstructure and Properties, Elsevier, 2017: pp. 23–57. https://doi.org/10.1016/B978-0-08-100270-4.00002-0.

[47] V.I. Danilov, V. v. Gorbatenko, L.B. Zuev, D. v. Orlova, L. v. Danilova, Luders deformation of low-carbon steel, Steel in Translation. 47 (2017) 662–668. https://doi.org/10.3103/S0967091217100035.

[48] J.F. Butler, Lüders front propagation in low carbon steels, J Mech Phys Solids. 10 (1962) 313–318. https://doi.org/10.1016/0022-5096(62)90003-0.

[49] N. Tsuchida, Y. Tomota, K. Nagai, K. Fukaura, A simple relationship between Lüders elongation and work-hardening rate at lower yield stress, Scr Mater. 54 (2006) 57–60. https://doi.org/10.1016/j.scriptamat.2005.09.011.

[50] T.B. Mező, P. Barkóczy, Study on Static Strain Aging Kinetics of High-Carbon Steel Wires and Its Impact on High-Strength Steel Cords, Metals (Basel). 11 (2021) 1684. https://doi.org/10.3390/met11111684.

[51] B.M. GONZALEZ, L.A. MARCHI, E.J. FONSECA, P.J. MODENESI, V.T.L. BUONO, Measurement of dynamic strain aging in pearlitic steels by tensile test, ISIJ International. 43 (2003) 428–432.

[52] A.K. Sachdev, Dynamic Strain Aging of Various Steels, Metallurgical Transactions A. 13 (1982) 1793–1797. https://doi.org/10.1007/BF02647835.

[53] H. Bhadeshia, R. Honeycombe, Formation of Martensite, in: Steels: Microstructure and Properties, Elsevier, 2017: pp. 135–177. https://doi.org/10.1016/b978-0-08-100270-4.00005-6.

[54] D.A. Porter, K.E. Easterling, Phase Transformations in Metals and Alloys, Springer US, Boston, MA, 1992. https://doi.org/10.1007/978-1-4899-3051-4.

[55] N. Dowling, Mechanical Behavior of Materials: Engineering methods for deformation, fracture and fatigue, 4th ed., Pearson, 2013.

[56] A.S.M.I.H. Committee, ASM Handbook, Volume 19 - Fatigue and Fracture, (1996). https://app.knovel.com/hotlink/toc/id:kpASMHVFF2/asm-handbook-volume-19/asm-handbook-volume-19.

[57] M. Kiani, G.T. Fry, Fatigue analysis of railway wheel using a multiaxial strain-based critical-plane index, Fatigue Fract Eng Mater Struct. 41 (2018) 412–424. https://doi.org/10.1111/ffe.12697.

[58] A. Kapoor, A re-evaluation of the life to rupture of ductile metals by cyclic plastic strain, Fatigue Fract Eng Mater Struct. 17 (1994) 201–219. https://doi.org/10.1111/j.1460-2695.1994.tb00801.x.

[59] J. Ahlström, B. Karlsson, Modified Railway Wheel Steels: Production and Evaluation of Mechanical Properties with Emphasis on Low-Cycle Fatigue Behavior, Metallurgical and Materials Transactions A. 40 (2009) 1557–1567. https://doi.org/10.1007/s11661-009-9846-9.

[60] D. Socie, B. Socie, Thermomechanical fatigue made easy, in: Fatigue, 2007.

[61] K. Bhanu Sankara Rao, B. Raj, Fatigue Testing: Thermal and Thermomechanical, in: Encyclopedia of Materials: Science and Technology, Elsevier, 2001: pp. 2999–3001. https://doi.org/10.1016/B0-08-043152-6/00534-9.

[62] T. BECK, P. HåHNER, H.-J. KüHN, C. RAE, A. E.E., H. ANDERSSON, A. KöSTER, M. MARCHIONNI, Thermo-mechanical fatigue – the route to standardisation (TMF-STANDARD), in: Novel Approaches to Improving High Temperature Corrosion Resistance, Elsevier, 2008: pp. 384–399. https://doi.org/10.1533/9781845694470.3.384.

[63] A. Esmaeili, M.S. Walia, K. Handa, K. Ikeuchi, M. Ekh, T. Vernersson, J. Ahlström, A methodology to predict thermomechanical cracking of railway wheel treads: From experiments to numerical predictions, Int J Fatigue. 105 (2017) 71–85. https://doi.org/10.1016/j.ijfatigue.2017.08.003.

[64] A. Haidari, P. Hosseini-Tehrani, Fatigue Analysis of Railway Wheels Under Combined Thermal and Mechanical Loads, Journal of Thermal Stresses. 37 (2014) 34–50. https://doi.org/10.1080/01495739.2013.850967.

[65] E. Affeldt, M.S. Loveday, C. Rinaldi Ricerca Sistema Energetico, Validated Code-of-Practice for Strain-Controlled Thermo-Mechanical Fatigue Testing, 2006. https://www.researchgate.net/publication/265152601.

[66] T. Vernersson, Temperatures at railway tread braking. Part 1: Modelling, Proc Inst Mech Eng F J Rail Rapid Transit. 221 (2007) 167–182. https://doi.org/10.1243/0954409JRRT57.

[67] T. Vernersson, Temperatures at railway tread braking. Part 2: Calibration and numerical examples, Proc Inst Mech Eng F J Rail Rapid Transit. 221 (2007) 429–442. https://doi.org/10.1243/09544097JRRT90.

[68] S. Teimourimanesh, T. Vernersson, R. Lundén, Modelling of temperatures during railway tread braking: Influence of contact conditions and rail cooling effect, Proc Inst Mech Eng F J Rail Rapid Transit. 228 (2014) 93–109. https://doi.org/10.1177/0954409712465696.

[69] M.S. Walia, A. Esmaeili, T. Vernersson, R. Lundén, Thermomechanical capacity of wheel treads at stop braking: A parametric study, Int J Fatigue. 113 (2018) 407–415. https://doi.org/10.1016/j.ijfatigue.2018.04.031.

[70] W. Hearn, Laser Based Powder Bed Fusion of Plain Carbon and Low-Alloy Steels: Microstructure and Processability, Licentiate thesis, Chalmers University of Technology, 2021.

[71] EOS GmBH, EOS M 100 Additive Manufacturing System for the Fast and Efficient Production of Delicate Metal Parts Metal Solutions, Munich, 2018. www.eos.info.

[72] C. Yildirim, Y. Zhang, E. Steyn, F. Liu, C. Detlefs, C. Jessop, J. Alström, Exploring Three-Dimensional Orientation and Residual Stresses in Railway Steels, in: TMS 2022, Anaheim, California, 2022.